

Investigation of two-beam-pumped noncollinear optical parametric chirped-pulse amplification for the generation of few-cycle light pulses

Daniel Herrmann,^{1,2,3,4*} Raphael Tautz,^{1,2,3,5} Franz Tavella,⁶
Ferenc Krausz,^{2,3} and Laszlo Veisz²

¹ These two authors contributed equally to this work.

² Max-Planck-Institut für Quantenoptik, Hans-Kopfermann-Strasse 1, 85748 Garching

³ Department für Physik, Ludwig-Maximilians-Universität München, Am Coulombwall 1, 85748 Garching, Germany

⁴ Present address: Lehrstuhl für BioMolekulare Optik, Department für Physik, Ludwig-Maximilians-Universität, Oettingenstrasse 67, 80538 München, Germany

⁵ Present address: Photonics and Optoelectronics Group, Department of Physics and Center for Nanoscience, Ludwig-Maximilians-Universität, Amalienstr. 54, 80799 München, Germany

⁶ HASYLAB/DESY, Notkestrasse 85, 22607 Hamburg, Germany

*Corresponding author: d.herrmann@physik.uni-muenchen.de

Abstract: We demonstrate a new and compact ϕ -plane-pumped non-collinear optical parametric chirped-pulse amplification (NOPCPA) scheme for broadband pulse amplification, which is based on two-beam-pumping (TBP) at 532 nm. We employ type-I phase-matching in a 5 mm long BBO crystal with moderate pump intensities to preserve the temporal pulse contrast. Amplification and compression of the signal pulse from 675 nm - 970 nm is demonstrated, which results in the generation of 7.1-fs light pulses containing 0.35 mJ energy. In this context, we investigate the pump-to-signal energy conversion efficiency for TBP-NOPCPA and outline details for few-cycle pulse characterization. Furthermore, it is verified, that the interference at the intersection of the two pump beams does not degrade the signal beam spatial profile. It is theoretically shown that the accumulated OPA phase partially compensates for wave-vector mismatch and leads to extended broadband amplification. The experimental outcome is supported by numerical split-step simulations of the parametric signal gain, including pump depletion and parametric fluorescence.

© 2010 Optical Society of America

OCIS codes: (190.7110) Ultrafast nonlinear optics; (190.4970) Parametric oscillators and amplifiers; (190.4975) Parametric processes; (320.7100) Ultrafast measurements; (230.4320) Non-linear optical devices; (260.7120) Ultrafast phenomena

References and links

1. D. Polli, M. R. Antognazza, D. Brida, G. Lanzani, G. Cerullo, and S. De Silvestri, "Broadband pump-probe spectroscopy with sub-10-fs resolution for probing ultrafast internal conversion and coherent phonons in carotenoids," *Chem. Phys.* **350**, 45-55 (2008).
2. T. Brabec and F. Krausz, "Intense few-cycle laser fields: Frontiers of nonlinear optics," *Rev. Mod. Phys.* **72**, 545-591 (2000).
3. F. Krausz and M. Ivanov, "Attosecond physics," *Rev. Mod. Phys.* **81**, 163-234 (2009).

4. K. Schmid, L. Veisz, F. Tavella, S. Benavides, R. Tautz, D. Herrmann, A. Buck, B. Hidding, A. Marcinkevičius, U. Schramm, M. Geissler, J. Meyer-ter-Vehn, D. Habs, and F. Krausz, "Few-Cycle Laser-Driven Electron Acceleration," *Phys. Rev. Lett.* **102**, 124801 (2009).
5. G. D. Tsakiris, K. Eidmann, J. Meyer-ter-Vehn, and F. Krausz, "Route to intense single attosecond pulses," *New J. Phys.* **8** (2006) 19.
6. A. Baltuška, Th. Udem, M. Uiberacker, M. Hentschel, E. Goulielmakis, Ch. Gohle, R. Holzwarth, V. S. Yakolev, A. Scrinzi, T. W. Hänsch, and F. Krausz, "Attosecond control of electronic processes by intense light fields," *Nature* **421**, 611-615 (2003).
7. R. Hörlein, Y. Nomura, D. Herrmann, M. Stafe, I. B. Földes, S. G. Rykovanov, F. Tavella, A. Marcinkevičius, F. Krausz, L. Veisz, and G. D. Tsakiris, "Few-cycle harmonic emission from solid density plasmas," (in preparation).
8. A. Dubietis, G. Jonusauskas, and A. Piskarskas, "Powerful femtosecond pulse generation by chirped and stretched pulse parametric amplification in BBO crystal," *Opt. Commun.* **88**, 437-440 (1992).
9. I. N. Ross, P. Matousek, G. H. C. New, and K. Osvay, "Analysis and optimization of optical parametric chirped pulse amplification," *J. Opt. Soc. Am. B* **19**, 2945-2956 (2002).
10. A. Dubietis, R. Butkus, and A. Piskarskas, "Trends in chirped pulse optical parametric amplification," *IEEE J. Sel. Top. Quantum Electron.* **12**, 163-172 (2006).
11. S. Witte, R. T. Zinkstok, A. L. Wolf, W. Hogervorst, W. Ubachs, and K. S. E. Eikema, "A source of 2 terawatt, 2.7 cycle laser pulses based on noncollinear optical parametric chirped pulse amplification," *Opt. Express* **14**, 8168-8177 (2006).
12. F. Tavella, Y. Nomura, L. Veisz, V. Pervak, A. Marcinkevičius, and F. Krausz, "Dispersion management for a sub-10-fs, 10 TW optical parametric chirped-pulse amplifier," *Opt. Lett.* **32**, 2227-2229 (2007).
13. D. Herrmann, L. Veisz, R. Tautz, F. Tavella, K. Schmid, V. Pervak, and F. Krausz, "Generation of sub-three-cycle, 16 TW light pulses by using noncollinear optical parametric chirped-pulse amplification," *Opt. Lett.* **34**, 2459-2461 (2009).
14. A. Dubietis, R. Danielius, G. Tamošauskas, and A. Piskarskas, "Combining effect in a multiple-beam-pumped optical parametric amplifier," *J. Opt. Soc. Am. B* **15**, 1135-1139 (1998).
15. A. Marcinkevičius, A. Piskarskas, V. Smilgevičius, and A. Stabinis, "Parametric superfluorescence excited in a nonlinear crystal by two uncorrelated pump beams," *Opt. Commun.* **158**, 101-104 (1998).
16. D. Brida, G. Cirmi, C. Manzoni, S. Bonora, P. Villoresi, S. De Silvestri, and G. Cerulo, "Sub-two-cycle light pulses at $1.6\mu\text{m}$ from an optical parametric amplifier," *Opt. Lett.* **33**, 741-743 (2008).
17. T. S. Sosnowski, P. B. Stephens, and T. B. Norris, "Production of 30-fs pulses tunable throughout the visible region by a new technique in optical parametric amplification," *Opt. Lett.* **21**, 140-142 (1996).
18. E. Žeromskis, A. Dubietis, G. Tamošauskas, A. Piskarskas, "Gain bandwidth broadening of continuum-seeded optical parametric amplifier by use of two pump beams," *Opt. Comm.* **203**, 435-440 (2002).
19. G. Tamošauskas, A. Dubietis, G. Valiulis, and A. Piskarskas, "Optical parametric amplifier pumped by two mutually incoherent laser beams," *Appl. Phys. B* **91**, 305307 (2008).
20. C. Wang, Y. Leng, B. Zhao, Z. Zhang, Z. Xu, "Extremely broad gain spectra of two-beam-pumped optical parametric chirped-pulse amplifier," *Opt. Commun.* **237**, 169-177 (2004).
21. R. L. Sutherland, 1996, *Handbook of Nonlinear Optics* (Marcel Dekker, New York).
22. G. Cerullo and S. de Silvestri, "Ultrafast optical parametric amplifiers," *Rev. of Sci. Instr.* **74**, 1-18 (2003).
23. V. G. Dmitriev, G. G. Gurzadyan, and D. N. Nikogosyan, *Handbook of Nonlinear Optical Crystals* (Springer, New York).
24. J. A. Armstrong, N. Bloembergen, J. Ducuing, and P. S. Pershan, "Interactions between light waves in a nonlinear dielectric," *Phys. Rev.* **127**, 1918-1939 (1962).
25. R. A. Baumgartner and R. L. Byer, "Optical Parametric Amplification," *IEEE J. of Quant. Electr.* **QE-15**, 432-444 (1979).
26. F. Tavella, A. Marcinkevičius, and F. Krausz, "Investigation of the superfluorescence and signal amplification in an ultrabroadband multiterawatt optical parametric chirped pulse amplifier system," *New J. Phys.* **8** (2006) 219.
27. A. Dement'ev, O. Vrublevskaia, V. Girdauskas, and R. Kazragyte, "Numerical Analysis of Short Pulse Optical Parametric Amplification Using Type I Phase Matching," *Nonl. Anal.: Modelling and Control* **9**, 39-53 (2004).
28. A. Kurtinaitis, A. Dementjev, and F. Ivanauskas, "Modeling of Pulse Propagation factor Changes in Type II Second-Harmonic Generation," *Nonl. Anal.: Modelling an Control* **6**, 51-69 (2001).
29. G. A. Reider, 1997, *Photonik* (Springer, New York).
30. L. Hongjun, Z. Wei, C. Guofu, W. Yishan, C. Zhao, and R. Chi, "Investigation of spectral bandwidth of optical parametric amplification," *Appl. Phys. B* **79**, 569576 (2004).
31. F. Tavella, K. Schmid, N. Ishii, A. Marcinkevičius, L. Veisz, and F. Krausz, "High-dynamic range pulse-contrast measurements of a broadband optical parametric chirped-pulse amplifier," *Appl. Phys. B* **3**, 753 (2005).
32. G. Arisholm, "General numerical methods for simulating second-order nonlinear interactions in birefringent media," *J. Opt. Soc. Am. B* **14**, 2543-2549 (1997).
33. S. Witte, R. T. Zinkstok, W. Hogervorst, and K. S. E. Eikema, "Numerical simulation for performance optimization of a few-cycle terawatt NOPCPA system," *Appl. Phys. B* **87**, 677684 (2007).

34. A. Picozzi and M. Haeltermann, "Influence of walk-off, dispersion, and diffraction on the coherence of parametric fluorescence," *Phys. Rev. E*, **63**, 056611-1 - 056611-11 (2001).
 35. A. Gatti, H. Wiedemann, L. A. Lugitao, and I. Marzoli, "Langevin treatment of quantum fluctuations and optical patterns in optical parametric oscillators below threshold," *Phys. Rev. A*, **56**, 877-897 (1997).
 36. D. A. Kleinmann, "Theory of Optical Parametric Noise," *Phys. Rev.*, **174**, 1027-1041 (1968).
 37. F. Salin, P. Georges, G. Roger, and A. Brun, "Single-shot measurement of a 52-fs pulse," *Applied Optics* **26**, 4528-4531 (1987).
 38. A. Brun, P. Georges, G. Le Saux, and F. Salin, "Single-shot characterization of ultrashort light pulses," *J. Phys. D: Appl. Phys.* **24**, 1225-1233 (1991).
 39. H. Mashiko, A. Suda, and K. Midorikawa, "All-reflective interferometric autocorrelator for the measurement of ultra-short optical pulses," *Appl. Phys. B* **76**, 525-530 (2003).
 40. R. Trebino, 2000, *Frequency-Resolved Optical Gating: The Measurement of Ultrashort Laser Pulses* (Kluwer Academic Publishers, Norwell, USA).
-

1. Introduction

Light pulses with duration of only a few optical cycles open up novel parameter regimes for a number of applications, ranging from time-resolved optical spectroscopy to high-field science [1, 2]. Progress in strong-field physics such as attosecond science [3] or laser-based particle acceleration [4] depend on the availability of suitable laser systems. Phase-controlled, intense, high-contrast, few-cycle light pulses can be used to generate powerful isolated attosecond pulses in the XUV range [5]. For this purpose, carrier-envelope phase effects with few-cycle pulses have been demonstrated [6, 7].

The invention of OPCPA offered the prospect of generating few-cycle laser pulses by providing sufficient gain and gain-bandwidth to approach the terawatt level [8, 9]. NOPCPA offers many advantages over chirped pulse amplifiers (CPA), such as a broad gain-bandwidth, high single-pass gain, wavelength tunability and low thermal effects [10]. Due to many challenges, amplification and compression of few-cycle, terawatt-class pulses have only recently been demonstrated in the near-infrared [11, 12, 13]. Few-cycle NOPCPA systems require accurate dispersion control during stretching and compression over a broad bandwidth, along with optimum phase-matching conditions, and a high quality picosecond pump laser. This is needed to achieve an efficient conversion, to ensure a good spatial signal profile and to provide a high temporal pulse contrast. It was shown, that one can minimize optical parametric fluorescence (OPF) and reach a high pulse contrast suitable for high-field physics via moderately pumped NOPCPA in combination with a strong seed in 5 mm long BBO type-I phase-matching [13]. OPCPA and OPA allow for the use of multiple pump beams, which is an important but so far unexploited feature for laser systems [10]. The reason for this promising attribute is, that the relative pump phases are not important and no interferometric phase alignment is needed since the phase difference between the signal and the pump pulses are taken away by the idler pulse, hence compensating for random differences between them [14, 15]. Neighboring spectral regions of the seed can be amplified by using multiple pump beams in individual phase-matching geometry. Thus, a broader amplified signal spectrum can be achieved compared to employing just one pump beam. TBP can also increase the repetition rate for high-power OPCPA systems. Alternative approaches to TBP-NOPCPA for the generation of 1-3 cycle pulses are one-beam-pumping (OBP) collinear OPCPA at degeneracy and cascaded NOPCPA employing angular detuning [16, 17]. Previous TBP experimental studies were exclusively done on narrowband NOPCPA without revealing all characteristics like conversion efficiency, broadband signal spectra, broadband signal compressibility, pump beam interference, signal beam quality and simulated gain (based on five nonlinear coupled wave equations including pump depletion and OPF) at the same time [14, 18, 19]. Theoretical broadband TBP-NOPCPA studies predicted broadband compression to be very challenging because of phase jumps due to the TBP scheme [20]. Moreover, TBP-NOPCPA needs to be investigated in detail before implementation of this

scheme in multi-terawatt laser systems [13]. This is the motivation for the present publication.

2. TBP-NOPCPA scheme and numerical simulation

NOPCPA involves phase-matching of the pump, signal and idler waves inside of a birefringent nonlinear optical crystal showing a second-order susceptibility. Phase-matching can be achieved by adjusting the phase-matching angles θ_{pm} , Φ and the noncollinear angle σ aiming for the minimum wave-vector mismatch [9, 21, 22]:

$$\Delta \mathbf{k}_l = \mathbf{k}_{p1} - \mathbf{k}_s - \mathbf{k}_{il} \quad \forall l = 1, 2, \quad (1)$$

where the index l separates the different pump and idler pulses. BBO is the favored nonlinear crystal material because of its high damage threshold, large nonlinearity and advantageous optical properties for broadband phase-matching [23].

OPCPA is described by the nonlinear coupled wave equations [21, 24, 25, 26] which need to be extended for describing TBP-NOPCPA:

$$\begin{aligned} \frac{\delta A_{s1}}{\delta z} + \sum_m \alpha_{s1m} \frac{\delta^m A_{s1}}{\delta t^m} + \frac{j\beta_{s11}}{r} \frac{\delta}{\delta r} \left(r \frac{\delta A_{s1}}{\delta r} \right) + \dots + \gamma_{s1} \frac{\delta A_{s1}}{\delta r} \\ = -j\kappa_{s1} A_{i1}^* A_{p1} e^{-j\Delta k_1 z} - j\kappa_{s2} A_{i2}^* A_{p2} e^{-j\Delta k_2 z} + \sqrt{\epsilon_{s1}} \xi_{s1}(z, t) \end{aligned} \quad (2)$$

$$\frac{\delta A_{i1}}{\delta z} + \sum_m \alpha_{i1m} \frac{\delta^m A_{i1}}{\delta t^m} + \frac{j\beta_{i11}}{r} \frac{\delta}{\delta r} \left(r \frac{\delta A_{i1}}{\delta r} \right) + \dots + \gamma_{i1} \frac{\delta A_{i1}}{\delta r} = -j\kappa_{i1} A_s^* A_{p1} e^{-j\Delta k_1 z} + \sqrt{\epsilon_{i1}} \xi_{i1}(z, t) \quad (3)$$

$$\frac{\delta A_{i2}}{\delta z} + \sum_m \alpha_{i2m} \frac{\delta^m A_{i2}}{\delta t^m} + \frac{j\beta_{i21}}{r} \frac{\delta}{\delta r} \left(r \frac{\delta A_{i2}}{\delta r} \right) + \dots + \gamma_{i2} \frac{\delta A_{i2}}{\delta r} = -j\kappa_{i2} A_s^* A_{p2} e^{-j\Delta k_2 z} + \sqrt{\epsilon_{i2}} \xi_{i2}(z, t) \quad (4)$$

$$\frac{\delta A_{p1}}{\delta z} + \sum_m \alpha_{p1m} \frac{\delta^m A_{p1}}{\delta t^m} + \frac{j\beta_{p11}}{r} \frac{\delta}{\delta r} \left(r \frac{\delta A_{p1}}{\delta r} \right) + \dots + \gamma_{p1} \frac{\delta A_{p1}}{\delta r} = -j\kappa_{p1} A_s A_{i1} e^{j\Delta k_1 z} \quad (5)$$

$$\frac{\delta A_{p2}}{\delta z} + \sum_m \alpha_{p2m} \frac{\delta^m A_{p2}}{\delta t^m} + \frac{j\beta_{p21}}{r} \frac{\delta}{\delta r} \left(r \frac{\delta A_{p2}}{\delta r} \right) + \dots + \gamma_{p2} \frac{\delta A_{p2}}{\delta r} = -j\kappa_{p2} A_s A_{i2} e^{j\Delta k_2 z} \quad (6)$$

where α_{s1m} , α_{i1m} and α_{p1m} are the dispersion coefficients with order m . β_{s11} , β_{i11} and β_{p11} are the diffraction coefficients at first order and (...) are the higher order terms [27, 28]. γ_{s1} , γ_{i1} and γ_{p1} are the spatial overlap coefficients due to the noncollinear geometry. κ_{s1} , κ_{i1} and κ_{p1} are the nonlinear coupling coefficients as a function of signal wavelength [29], Δk_l is the wave-vector mismatch given by Eq. (1) and z is the direction of propagation.

If there is no input idler present ($A_{i1} = A_{i2} = 0$), the initial idler phase Φ_{il} self-adjusts to achieve maximum initial pump to signal and idler conversion efficiency for each pump-signal interaction separately. This leads to the generalized phase $\Omega(z=0)$ at the crystal input:

$$\Omega(0) = \Phi_{p1}(0) - \Phi_s(0) - \Phi_{il}(0) = -\frac{\pi}{2} \quad \forall l = 1, 2. \quad (7)$$

In the presence of wavevector mismatch $\Delta\mathbf{k}_l$, there is an accumulated phase $|\Delta\mathbf{k}_l L|$ with propagation distance. Consequently, the phases of the waves have to change to maintain the $\Omega = -\pi/2$ criteria (Eq. (7)). This means, that an additional phase will be imprinted on the signal wave during amplification. The phase terms $\Phi_{p1,p2,s,i1,i2}$ for the pump waves, signal wave and idler waves can be obtained by solving the imaginary part of the coupled wave equations (Eq. (2-6)) and using the Manley-Rowe-relation. If the input signal intensity is small compared to the input pump intensity, i.e. in case of low pump depletion, one can obtain a good approximation for the signal phase at the output for each isolated pump-signal interaction separately (i.e. one pump beam is blocked at this time) [9]:

$$\Phi_{sl}(z=L) = \Phi_s(0) - \frac{\Delta k_l L}{2} + \arctan\left\{\frac{\Delta k_l \times \tanh\left[\left[g_l^2 - (\Delta k_l/2)^2\right]^{1/2} L\right]}{2\left[g_l^2 - (\Delta k_l/2)^2\right]^{1/2}}\right\} \quad \forall l = 1, 2, \quad (8)$$

where $g_l = 4\pi d_{eff} \sqrt{I_{pl}(0)/(2\epsilon_0 n_{p1} n_s n_{i1} c \lambda_s \lambda_{i1})}$ is the gain coefficient and

$$d_{eff} = d_{31} \sin\theta_{pm} - d_{22} \cos\theta_{pm} \sin 3\phi_l \quad \forall l = 1, 2 \quad (9)$$

is the effective nonlinear coefficient. Since the accumulated signal phase Φ_{sl} depends on the pump intensity, a shot-to-shot variation of the carrier-envelope phase (CEP) is possible in the parametric amplifier, if the pump intensity is not constant in time. A maximum phase-slippage of π over the crystal length L is acceptable for a coherent built-up of the amplified signal in the small signal gain regime [22, 30]. This defines a criteria for the parametric bandwidth and leads to:

$$|\Delta\mathbf{k}_l L| \leq \pi \quad \forall l = 1, 2. \quad (10)$$

We choose the TBP-NOPCPA geometry shown in Fig.2(a), to ensure optimum type-I phase-matching. In this setup, the critical phase-matching angle θ_{pm} can be kept the same for both pump-signal interactions, whereas the internal noncollinear angle σ_l is adjusted for both interactions individually to achieve the broadest amplified signal spectrum. The two pump beams are located in the ϕ -plane, which is perpendicular to the critical phase-matching plane (θ -plane). The change of d_{eff} due to the deviation of the non-critical phase-matching angle ϕ_l for the individual interactions is negligible but nevertheless was taken into account for the numerical simulations.

This TBP-NOPCPA setup is essentially different from conventional type-I NOPCPA geometries, where the so-called tangential phase-matching or the Poynting vector walk-off compensation phase-matching are used. In these cases, the pump and signal beam are located in the θ -plane. In this conventional configuration, it would not be possible to achieve a TBP geometry, where the two separate pump beams have the same phase-matching angle θ_{pm} and the noncollinear angles σ_l can be changed without changing θ_{pm} .

We perform symmetrized numerical split-step simulations of NOPCPA [26, 28, 32, 33] with the extension to the TBP scheme and including quantum noise field terms $\epsilon_{s1,il} \xi_{s1,il}(z,t)$ into the coupled wave equations (Eq. (2-6)) [34]. The complex stochastic variables $\xi_{s1,il}(z,t)$ have a Gaussian distribution with a zero mean value $\langle \xi_{s,il}(z,t) \rangle = 0$ and the correlation $\langle \xi_q(z,t) \xi_r^*(z',t') \rangle = \delta_{q,r} \delta(z-z') \delta(t-t')$ [35]. $\epsilon_{s1,il}$ are the noise intensities of the signal and the idler waves. The spatial overlap coefficient for the signal γ_{s1} is set to zero as the signal propagates normal to the crystal plane. We perform the parametric amplification in the time domain within the so-called *nonlinear step* (Eq. (2-6)) for the amplitudes of the signal wave, the OPF in the signal direction, the idler waves, the OPF in the idler directions and the pump waves. For the pump pulses we employ the measured beam shapes: a 6th-order super-Gaussian beam in space and a Gaussian pulse in time. In case of the seed, we use a Gaussian pulse in time and space as approximation. As further input parameters, we take measured seed and pump

characteristics prior to amplification. We choose an unamplified seed spectrum ranging from 650 nm until 1060 nm in the simulation to reveal the maximum parametric gain bandwidth. The temporal delays between seed pulse and each pump pulse are chosen to achieve best match between simulation results and experimental outcome. For the broadest signal spectrum, we choose $\sigma_1 = 2.22^\circ$, $\sigma_2 = -2.16^\circ$ and $\theta_{pm} = 23.62^\circ$. The wavevector mismatch Δk is assumed to be zero only for the OPF. This approximation is considered valid, since the transition rate from the pump photon to signal and idler photon is highest in the direction of smallest phase-mismatch and consequently only in this case efficient amplification of OPF is possible from the quantum noise level [26, 36].

Dispersion, diffraction and spatial overlap due to the noncollinearity for the TBP-NOPCPA process is taken into account in the *linear step*. For the dispersion we expand the spectral phase $\Delta\varphi_{s1,pl,il}(\omega)$ in a Taylor series until 4th order, including group velocity mismatch, and apply it in the frequency domain involving the Fourier transform \mathcal{F} :

$$A_{s1,pl,il}(r, z + \Delta z, t) = \mathcal{F}^{-1} \{ \mathcal{F} [A_{s1,pl,il}(z, t)] e^{j\Delta\varphi_{s1,pl,il}(\omega)} \} \quad \forall 1 = 1, 2. \quad (11)$$

For the diffraction (diff) and spatial overlap due to the noncollinearity (nc), we include a spatial phase term $\Delta\varphi_{s1,pl,il}^{spatial} = \Delta\varphi_{s1,pl,il}^{nc} + \Delta\varphi_{s1,pl,il}^{diff}$ by applying the linear Fourier step to the transposed data matrices [26, 27]:

$$A_{s1,pl,il}^\dagger(r, z + \Delta z, t) = \mathcal{F}^{-1} \{ \mathcal{F} [A_{s1,pl,il}^\dagger(z, t)] e^{j\Delta\varphi_{s1,pl,il}^{spatial}} \} \quad \forall 1 = 1, 2. \quad (12)$$

We perform the numerical model, based on Eq. (2-6) and Eq. (11), (12) with 500 split-step iteration loops for a 5 mm long type-I BBO crystal.

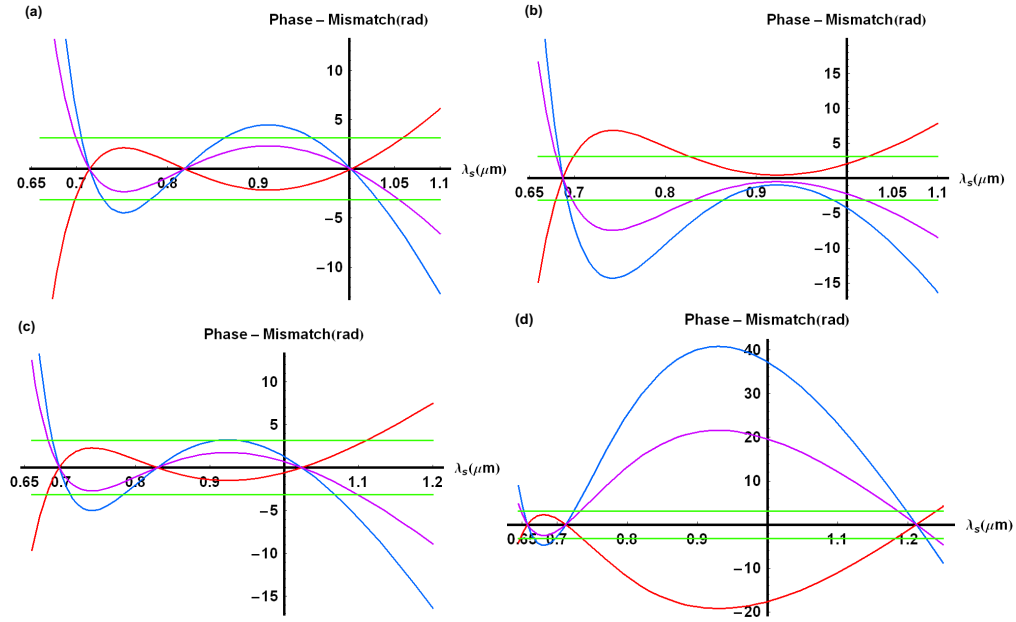


Fig. 1. Wave-vector mismatch $\Delta k_L L$ (blue), OPA-phase $\Phi_{st}(z=L)$ (red), sum of both (purple) and $\Delta k_L L = \pm\pi$ (green) for the cases of (a) $\sigma = 2.22^\circ$, $\theta_{pm} = 23.62^\circ$, $L=5$ mm, $\lambda_p=532$ nm (b) $\sigma = 2.16^\circ$, $\theta_{pm} = 23.62^\circ$, $L=5$ mm, $\lambda_p=532$ nm (c) $\sigma = 2.155^\circ$, $\theta_{pm} = 23.55^\circ$, $L=3$ mm, $\lambda_p=532$ nm and (d) $\sigma = 2.04^\circ$, $\theta_{pm} = 23.62^\circ$, $L=5$ mm, $\lambda_p=515$ nm

To directly show, outside the numerical simulations, which spectral components can be amplified in TBP-NOPCPA employing 5 mm long BBO type-I phase-matching, we calculate the

wave-vector mismatch by using Eq. (1) and the signal phase through Eq. (8) separately for each pump-signal interaction (i.e. while the other pump beam is blocked). The results are shown in Fig. 1(a) and (b). According to Eq. (10), the spectral components between 675 nm and 1050 nm can be amplified in case of TBP-NOPCPA (Fig. 1(a) and (b)) and between 700 nm and 1050 nm in case of broadband OBP-NOPCPA (Fig. 1(a)). This is in agreement with the measured signal spectra shown in Fig. 4, where the unamplified seed spectrum ranges from 650 nm until 970 nm. Moreover, Fig. 1 shows, that the signal phase Φ_{sl} accumulated over the crystal length L partially compensates for wave-vector mismatch $\Delta k_l L$ and pushes the overall phase-mismatch for the amplified spectral components below the limit in Eq. (10) for each individual pump-signal interaction. Maximum amplification is achieved, if the criterion for the general phase (Eq. (7)) is fulfilled. If there is no idler present at the beginning of the amplification, the idler phase self-adjusts to maximize the gain. During amplification however, the wave-vector mismatch (Eq. (1)) forces the phases of the waves to maintain this criterion. Nevertheless, we want to emphasize, that it remains to be theoretically investigated, how the total wave-vector mismatch and the total signal phase evolve, if both pump beams are present in the crystal. Nevertheless, the amplified spectra in Fig. 4 show, that the latter unknown effect does not noticeably change the phase-matched bandwidth compared to taking the phase-mismatch for each pump-signal interactions separately and applying the criterion for amplification in Eq. (10) afterwards. This approach is even exact for spectral regions in Fig. 4(b), where amplification is only due to one pump beam; i.e. for $\leq \sim 700$ nm and for ~ 700 nm-800 nm.

In principle, such a broad spectrum from 675 nm to ≥ 1050 nm can also be amplified with a similar gain using a 3 mm long BBO crystal in OBP-NOPCPA geometry, pumped with about 3 times higher intensity at 532 nm (Fig. 1(c)). Unfortunately, such an approach would lead to increased OPF and reduced temporal pulse contrast eventually not suitable for high-field physics [26, 31]. Moreover, such a high pump intensity is above the BBO damage threshold for this pump pulse duration. High contrast amplification of sub-three-cycle, TW light pulses was previously demonstrated using 5 mm long type-I BBO at moderate pump intensities [13]. Moreover, investigations on TBP-NOPCPA are also of high interest for multiple-color-pumping. For instance, one can perform pumping it with the second-harmonic of Nd:YAG and with the second-harmonic of Yb:YAG (at 515 nm) in the same NOPCPA stage to enhance the signal spectrum. A proposed phase-matching for this case is shown in Fig. 1(a) and (d). For example, the important question has to be answered, if a signal spectrum consisting of disjunct spectral components amplified by different pump beams can actually be compressed. The compressibility of such a spectrum is shown in the present investigations.

3. Experimental setup

The experimental TBP-NOPCPA set up is shown in Fig. 2(b). We use a part of the setup of a sub-three-cycle, 16-TW NOPCPA laser system described in Ref. [13], which is used for high-field experiments such as high-order harmonic generation from overdense plasmas and electron acceleration [7, 4]. As seed source for the TBP-NOPCPA we use 2 μ J pulses with a spectrum ranging from 650 nm to 970 nm (see Fig. 4(a)) and a FWHM pulse duration of 22 ps at 10 Hz repetition rate. The seed is negatively chirped by using a reflection grism-pair and an acousto-optic modulator (Dazzler, Fastlite). The group delay between the spectral boundaries of the stretched seed is 42 ps. The pump pulses for the TBP-NOPCPA are generated with a commercial Nd:YAG laser amplifier (Ekspla), which provides up to 1 J pulses at 532 nm with a FWHM pulse duration of 78 ps at 10 Hz repetition rate. The seed and pump pulses are synchronized in an all-optical way. The TBP-NOPCPA stage consists of a 5 x 5 x 5 mm³ type-I BBO crystal and is pumped with variable total pump energy up to 12 mJ in two beams. The pump beam is relay imaged from the pump laser output on the BBO crystal and split into two parts (pump

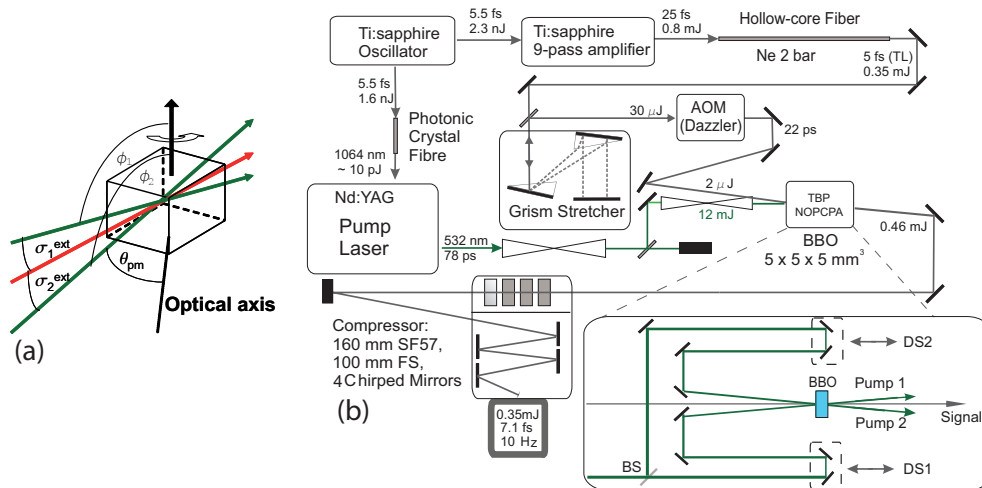


Fig. 2. (a) Optical schematic of the TBP-NOPCPA phase-matching geometry. (b) Layout of the TBP-NOPCPA experimental set up: BS - beamsplitter, DS - delay stage, AOM - acousto-optic modulator.

1 and pump 2) with a 50%:50% beamsplitter. Each pump beam has its own delay stage to achieve temporal overlap between the pump pulses and the seed pulse. The amplified signal beam is expanded from about 2 mm to 18 mm and compressed in bulk material consisting of 160 mm SF57 (Schott) and 100 mm fused silica. After the bulk compressor, the beam is down-collimated to about 6 mm and led into a vacuum compression chamber for final compression with 4 positive-dispersion chirped mirrors. The stretcher and compressor together have a calculated B-integral of 0.08 and the compressor has a throughput of 75% (including several silver mirrors).

The pulse duration is measured with a home-built all-reflective single-shot second-order autocorrelator, which is described in section 4.

4. All-reflective single-shot second-order intensity autocorrelator for few-cycle pulse characterization

Single-shot autocorrelation set ups have been demonstrated many years ago [37][38], as well as all-reflective multi-shot autocorrelators being able to measure pulse durations of only a few femtoseconds [39]. To our knowledge, up to now no all-reflective single-shot second-order intensity autocorrelator was realized and used to characterize light pulses with a duration of only a few cycles and a spectral bandwidth exceeding 300 nm. The following presented set up was specially designed to measure the duration and intensity distribution of the pulses generated in Ref. [13] and in the present experiment.

Figure 3 shows the set up of our home-built all-reflective single-shot second-order intensity autocorrelator. The main feature of this device is its minimized dispersion as well as the temporal resolution of about 197 attoseconds, which allows the characterization of few-cycle light pulses. A broad spectral range, from 675 nm up to 1000 nm, made the realization to a major challenge.

The set up consists of two irises at the entrance of the autocorrelator allowing an accurate alignment of the incoming beam. For splitting the beam in two identical replicas, geometric beamsplitting is used, which is done by a D-shaped mirror. This method is used to minimize dispersion in the optical path of the fundamental pulses. Due to the broad spectrum of few-

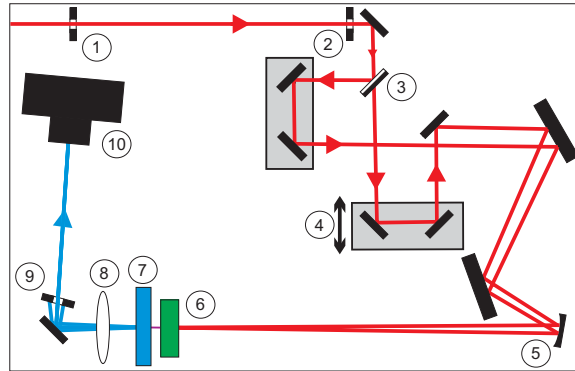


Fig. 3. Setup of the single-shot all-reflective second-order intensity autocorrelator with a temporal resolution of about 197 as/px and an observation window of 565 fs. 1 & 2: entrance iris, 3: geometric beamsplitter, 4: delay stage with micrometer screw, 5: cylindrical mirror, 6: SHG crystal, 7: color-glass filter, 8: achromatic imaging lens, 9: small aperture iris, 10: CCD detector (Larry 3000 USB)

cycle pulses even thin dispersive elements, like plate beam-splitters, would cause significant distortion of the original pulse. Pellicle beam-splitters are not chosen because of their sensitivity to vibrations. The upper part of the beam propagates in forward direction into the delay stage, whereas the lower part of the beam is deflected by 90° . In single-shot devices, the delay stage is only used for finding the zero-delay at the intersection point in the nonlinear optical crystal and for calibration. Unlike in a multi-shot autocorrelator the two pulse replicas are overlapped in the nonlinear optical crystal under a horizontal noncollinear angle of $\sigma_{nc} = 2.34^\circ$. A cylindrical mirror with a focal length of 300 mm placed in front of the crystal generates line foci in the horizontal plane with a vertical diameter of about $51 \mu\text{m}$. This method drastically reduces the required pulse energy to $10 \mu\text{J}$. With a phase-matching angle $\Theta_{pm} = 42^\circ$ and a thickness of the BBO crystal of $5 \mu\text{m}$, type-I phase-matching for the whole spectral bandwidth of the fundamental is provided, which allows phase matching starting at 465 nm and exceeding 1100 nm. The wavelength which has perfect phase matching was chosen to be 583 nm. The deviation from the laser central wavelength, located at 790 nm, allows a better phase matching in the short wavelength region while maintaining acceptable phase matching at long wavelengths.

For alignment purpose, the fundamental light is blocked behind the BBO crystal with a BG37 color glass filter. The second harmonic signal is then imaged by an achromatic lens with a focal length of 40 mm and four-time magnified from the crystal plane to the detector. The detector is a linear CCD array (Larry 3000 USB, Ames Photonics) with 3000 pixels in a horizontal row and a width of $7 \mu\text{m}$ each. In the focal plane of the imaging lens, the two second harmonic signals, propagating in direction of the fundamental beams, are blocked by a small aperture to prevent deteriorations of the autocorrelation signal. The isolated second harmonic photons at the bisector of the noncollinear angle σ_{nc} , carrying the intensity autocorrelation function in their transversal spatial intensity profile, are recorded by the detector mentioned above. An additional BG37 color glass filter reduces fundamental stray light reaching the detector.

The temporal resolution and observation window, being the two important properties, are defined by the maximum width of the signal, which is limited by the aperture of the BBO crystal $d = 5 \text{ mm}$, and the noncollinear angle σ_{nc} . Using basic geometry, the temporal observation window τ_{obs} can be expressed by

$$\tau_{obs} = \frac{n \cdot d \cdot \sin(\sigma_{nc}/2)}{c} \quad (13)$$

where c denotes the velocity of light in vacuum and n the ordinary refractive index of BBO at 790 nm. For $\sigma_{nc} = 2.34^\circ$ used in the setup, the obtained observation window has a size of $\tau_{obs} = 565$ fs (Eq. (13)). The CCD array with a width of 21 mm, containing 3000 pixels, records a four-times magnified image of the signal with an extension of 20 mm. Hence, the achieved temporal resolution r_{AC} results in the observation window divided by the number of pixels, covered by the signal, and has a value of $r_{AC} = 197 \frac{as}{px}$ for $\sigma_{nc} = 2.34^\circ$.

To estimate the absolute error of the pulse duration measured with the autocorrelator, the single errors have to be investigated. The pulse duration observed by autocorrelation consists of three variables

$$\tau_{pulse} = \frac{\tau_{AC} \cdot r_{AC}}{K} \quad (14)$$

where K denotes the deconvolution factor, τ_{AC} the FWHM of the autocorrelation trace in pixels and r_{AC} the temporal resolution of $197 \frac{as}{px}$ as mentioned above. The FWHM pulse duration (Eq. (14)) is obtained by dividing the temporal FWHM of the autocorrelation trace ($\tau_{AC} \cdot r_{AC}$) by the deconvolution factor K . This value is unique and strongly dependent on the pulse shape and hence strongly influences the measurement error. We calculated the deconvolution factor for the Fourier transformed pulses of several different spectra of our TW laser system, ending up with a value of $K = 1.35 \pm (1 \cdot 10^{-3})$. The change in the converted spectrum by the phase-matching curve of the BBO crystal has also been considered in this calculation.

Fortunately, in single-shot SHG autocorrelation measurement no geometrical distortions occur, since the generated second harmonic signal propagates along the bisector of angle formed by the input beams. Consequently there are no geometrical effects, decreasing the accuracy of the measurement [40].

An error originating from the calibration Δr_{AC} was calculated to be $4 \frac{as}{px}$, while an error of τ_{AC} could be reduced by interpolation to $\Delta \tau_{AC} = 0.1$ px.

Gaussian error propagation consequently leads to a total error of 0.12 fs for a fourier limited pulse. The deviation of the measured pulse from the Fourier limited pulse duration causes some deviation of the deconvolution factor K . Consequently the measurement error is influenced by this deviation which is hard to estimate, but as pulse duration gets close to the transform limit this error is also supposed to become very small.

For measuring the pulses of our present set up, the beam was coupled out of the compressor chamber through a 3 mm thick fused silica window. In addition to the window and some air, further dispersion of about 40 fs^2 is caused by reflections from seven protection-coated silver mirrors and the $5 \mu\text{m}$ thick BBO crystal inside the autocorrelator. Of course this dispersion is compensated by the AOM when measuring the optimized pulse duration.

Altogether the presented all-reflective single-shot second-order intensity autocorrelator was specially designed to characterize few-cycle pulses. With a temporal observation window of 565 fs and a temporal resolution of about 197 as, it is well suited to measure duration and intensity distribution of few-cycle pulses at realtime with a repetition rate of 10 Hz given by the laser system.

5. Results and discussion

The seed is amplified in the TBP-NOPCPA geometry shown in Fig. 2(a) and a signal energy up to 0.46 mJ is achieved. The broadest measured signal pulse spectrum is shown in Fig. 4(b). The signal pulse spectrum ranges from 675 nm to 970 nm leading to a Fourier limit of 6.7 fs. The TBP setup was modified to operate it also as OBP-NOPCPA with the same total pump energy by replacing the beamsplitter with a mirror. A typical signal spectrum in the OBP-NOPCPA case is shown in Fig. 4(a). This spectrum ranges from around 700 nm up to 970 nm leading to a Fourier limit of 8.5 fs. The spectral limits in Fig. 4(b) at low wavelength (675 nm and 700

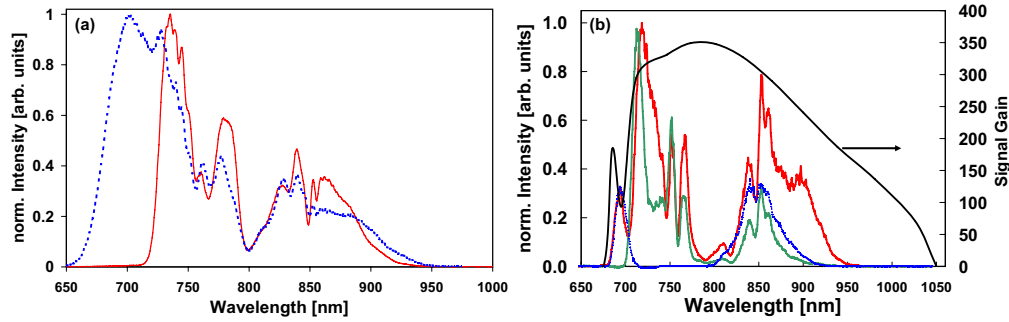


Fig. 4. (a) Unamplified seed spectrum (blue dotted) and amplified signal spectrum (red) in case of OBP-NOPCPA by phase-matching almost the same bandwidth as in Ref. [13] with $\sigma = 2.23^\circ$ and $\theta_{pm} = 23.62^\circ$. (b) Amplified signal spectrum using the TBP-NOPCPA scheme (red) with $\sigma_1 = 2.22^\circ$, $\sigma_2 = -2.16^\circ$ and $\theta_{pm} = 23.62^\circ$, the corresponding simulated gain (black), amplified signal spectrum using only pump1 (green) and using only pump2 (blue dotted).

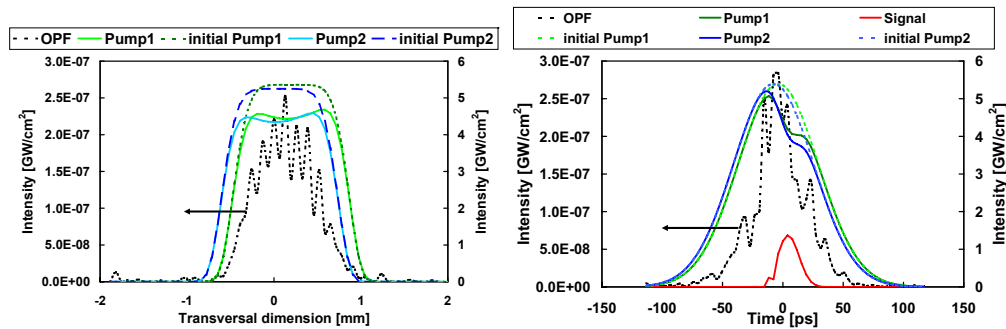


Fig. 5. Initial pump pulses and pump, signal and OPF after amplification in the time and space domain.

nm) are due to the different phase-matching geometry (see Fig. 1) and at the long wavelength are due to a lack of seed components above 970 nm, although amplification is theoretically possible up to 1050 nm (Fig. 4(b)). The dip in the signal spectra at around 800 nm results from the corresponding dip in the unamplified seed spectrum, which is a consequence of the self-phase modulation taking place in the hollow-core fiber.

Figure 4(b) shows the spectral parametric signal intensity gain obtained with the numerical split-step simulation described in section 2. The simulated amplified signal energy content is 0.49 mJ distributed over a spectral bandwidth from 675 nm to 970 nm, which matches the experimental values. Our simulations show an OPF peak intensity of $2.8 \cdot 10^{-7} \text{ GW/cm}^2$ and a signal peak intensity of 1.4 GW/cm^2 after amplification. This leads to an expected pulse contrast ratio of $6 \cdot 10^{-11} - 10^{-10}$ on the picosecond timescale after compression, assuming the beam transport efficiency and compressor transmission to be the same for signal and OPF. The OPF after amplification in space and time relative to the pump pulses and the signal pulse at the end of the BBO crystal is shown in Fig. 5. OPF does only occur within the temporal and spatial window of the pump pulse and shows strong amplitude modulation in the time and space domain.

Additionally, we measure the signal energy as function of pump intensity and calculate the energy pump-to-signal conversion efficiency. The results are shown in Fig. 6(a). For this rea-

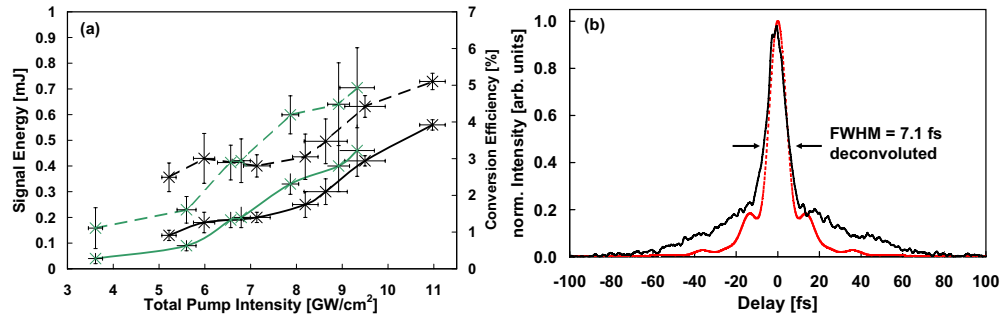


Fig. 6. (a) The dotted curves show the TBP-NOPCPA pump-to-signal conversion efficiency for the case of the red signal spectrum shown in 4(b) (green) and for the case of the signal spectrum similar to the red curve shown in 4(a)(black) with $\sigma_1 = -\sigma_2 = 2.23^\circ$ and $\theta_{pm} = 23.62^\circ$. The solid curves show the corresponding signal energy as function of total pump intensity. (b) Measured second-order single-shot autocorrelation (solid black curve) and calculated autocorrelation trace (red dotted curve)

son, we are able to investigate, if the phase-matching ($\sigma_1 = -\sigma_2 = 2.23^\circ$ and $\theta_{pm} = 23.62^\circ$) for the TBP-NOPCPA geometry aiming for a spectrum similar to one also achievable with OBP-NOPCPA (the case of Fig. 4(a)) is comparable to the conversion efficiency of the TBP-NOPCPA phase-matching geometry in case of Fig. 4(b) with broader amplified bandwidth. As result, the conversion efficiency is comparable within the error bars for both cases. Moreover, we measure the pulse duration of the amplified and compressed broadband signal pulse via an all-reflective second-order single-shot autocorrelation. The results are shown in Fig. 6(b) and reveal a FWHM pulse duration of 7.1 fs, whereas the Fourier-limited FWHM pulse duration is typically 6.7 fs. Consequently, compression is achieved to within 6% of the FWHM Fourier-limit. This important fact reveals the compressibility of the whole amplified signal bandwidth, although this signal spectrum is composed of two individual NOPCPA interactions taking place in the same nonlinear crystal. A deconvolution factor of 1.4 is calculated from the spectrum. TBP-NOPCPA also makes an additional spectral shaping possible compared to OBP-NOPCPA; i.e. shaping of the steep edge at 700 nm in the amplified signal spectrum in Fig. 4(a). This can potentially prevent pulse satellites from occurring after compression if a saturated TBP-NOPCPA stage is used, which would be present due to a sharp spectral edge even in case of compression close to the Fourier-limit [11, 12, 13]. In this case, a better pulse contrast is achievable due to an improvement of the foot of the compressed pulse, using a saturated amplifier stage.

Furthermore, there have been concerns, that a transient grating generated by the intersecting pump beams could potentially degrade the signal beam quality, since the amplification strongly depends on the pump intensity. For this reason, we investigate if there is an intensity grating (due to interference) present inside the BBO crystal and whether this grating negatively affects the signal beam quality. For this purpose, we image the BBO crystal plane with an achromatic lens onto a CCD camera with a pixel size of $6.7 \times 6.7 \mu m^2$. We magnify the object with a calibrated factor of 11 and verify, that crystal defects in the crystal are sharp on the CCD image in any case.

Firstly, we imaged only the intersection of the two pump beams and recorded the magnified crystal plane as a function of relative polarization orientation of the two beams. In this case, the seed was blocked before the crystal. The images and their lineouts are shown in Fig. 7(c) and (a), where 0° denotes parallel polarization orientation of the two pump beams and 90° corresponds to orthogonal relative polarization orientation. We found, that if the polarization of the two pump beams is parallel to each other and thus allow for interference taking place,

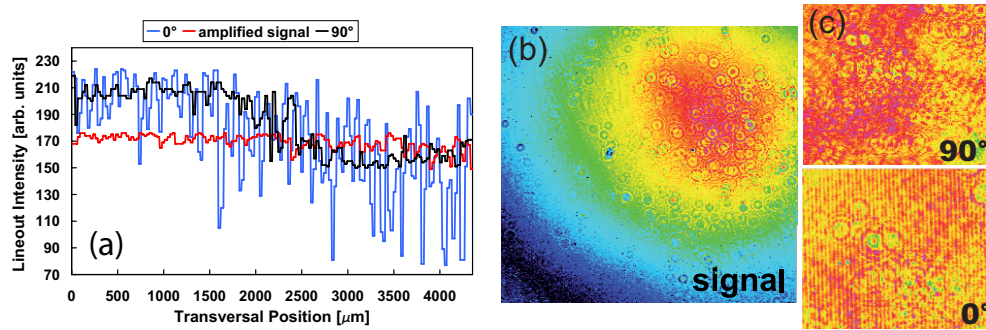


Fig. 7. Image of the BBO crystal plane magnified by factor 11 on a CCD camera: (a) Image line outs of the crystal plane. (b) Image of the amplified signal beam profile. (c) Image of the intersecting pump beam profiles in the crystal plane with varying relative polarization orientation: (0° denotes parallel, 90° denotes orthogonal polarization of the two pump beams).

there is clearly a pump intensity modulation present (see Fig. 7) in the crystal plane with a period of $\sim 7\mu\text{m}$, taking the magnification factor into account. This modulation vanishes in case of orthogonal polarization between the two pump beams, because then there is no interference possible. Consequently, this optical set up is able to resolve an intensity grating due to interference inside the BBO crystal.

Secondly, we unblocked the seed and measured the magnified image of the amplified signal in the crystal plane, while the pump beams are blocked after passing through the crystal. Figure 7(b) and (a) show, that we observed no signal intensity modulation due to the pump interference in the beam profile and the corresponding lineout. This can be explained as follows:

The transient grating due to the interference between the two pump beams inside the BBO crystal evolves on the angle bisector in between the pump beams. Since the two noncollinear angles are not the same, the signal beam traverses this bisector leading to a transversal shift with respect to the bisector of half a grating period over the crystal length. Consequently, this smearing effect can prevent the pump grating from degrading the signal beam quality. Apart from general noncollinear smearing, other effects like the Poynting vector walk-off can also contribute to this effective smearing.

6. Conclusion

We outlined a new concept (TBP-NOPCPA) for the generation of few-cycle, high-contrast, multi-terawatt light pulses. Moreover, the present experiment demonstrated compressibility of an amplified signal pulse, whose spectral components result from amplification by two separate pump beams in the same nonlinear crystal. In this context, we experimentally showed amplification and compressibility of the signal between 675 nm and 970 nm leading to 7.1-fs, 0.35-mJ light pulses after compression to within 6% of the FWHM Fourier-limit. Technical details of few-cycle pulse characterization are outlined. We investigated geometry, phase-mismatch, signal gain bandwidth, pump-to-signal conversion efficiency and signal beam quality for this new broadband ϕ -plane-pumped TBP-NOPCPA scheme. Additionally, we performed numerical split-step simulations of TBP-NOPCPA to obtain the parametric gain curve and to study the level of OPF. The temporal pulse contrast ratio was simulated to be around 10^{-10} on ps timescales after amplification and compression. It was shown that the accumulated OPA phase partially compensates for wave-vector mismatch to maintain

maximum gain and leads to extended broadband amplification. Summing up, the present investigations revealed, that TBP-NOPCPA is a promising parametric scheme without a decrease in amplified signal compressibility, amplified signal beam quality and conversion efficiency, compared to conventional one-beam-pumping NOPCPA. The presented theoretical considerations and numerical simulations showed, that amplification is possible between 675 nm and 1050 nm in a 5 mm long BBO crystal. Consequently, high-contrast, sub-7-fs, multi-TW pulses are achievable with a 5 mm long type-I BBO crystal, pumped at 532 nm, in case of TBP-NOPCPA.

Acknowledgements

This work was supported by Deutsche Forschungsgemeinschaft (contract TR18), the association EURATOM-Max-Planck-Institut für Plasmaphysik and by the Cluster of Excellence Munich center for Advanced Photonics (MAP). D. H., who mainly worked on experimental and theoretical TBP-NOPCPA, is also grateful to Studienstiftung des deutschen Volkes. R. T., who mainly worked on pulse diagnostics and the seed source, is thankful to Deutsche Forschungsgemeinschaft (contract TR18).